Double-pass imaging background-oriented schlieren technique for focusing on measurement target

Y. Hirose[1] · M. Yamagishi[2] · S. Udagawa[3] · T. Inage[4] · Y. Tagawa[5] · M. Ota[2]

Abstract

This paper introduces the double-pass imaging background-oriented schlieren (DPBOS) technique to overcome a defocusing problem of conventional background-oriented schlieren (BOS) systems. In the conventional BOS system, a camera focuses on a background situated behind a measurement target, which inevitably causes a blurred image of the target. The advantage of the proposed technique, using a digital projector with proper optical alignment, is that the camera focuses on both the target and the background image at the same time. Therefore, measurement in the vicinity of the target can be achieved with higher sensitivity than that of the conventional BOS system. For validation, a test target (lens) and the density field near a heat sink are measured using the DPBOS. The results show good agreement with theoretical prediction and exhibit higher sensitivity than the conventional and telecentric BOS system. In addition, the accuracy of DPBOS was assessed by comparing the calculated surface temperatures from the displacement of DPBOS and conventional BOS with the corresponding theoretical temperature. As the results, the DPBOS and conventional BOS have errors of 3% and 9%, respectively. The proposed method clearly shows the advantage of DPBOS over BOS in overcoming the defocus problem and achieving high-accuracy measurements.

1 Introduction

The background-oriented schlieren (BOS) technique proposed by Meier (Meier 2002) enables quantitative density measurements of flow fields using computer-aided image analysis. This technique has many advantages, and it can be used in a wide range of applications such as supersonic wind-tunnel measurement with scale models, underwater shockwaves, real-scale model measurement, and droplets caused by coughing when wearing a face mask (Raffel 2015;

✉ M. Ota
  ota@faculty.chiba-u.jp

1 Mechanical & Electronic Engineering, Salesian Polytechnic, Tokyo 1940215, Japan

2 Graduate School of Engineering, Chiba University, Chiba 2638522, Japan

3 Aerospace Engineering Course, Tokyo Metropolitan College of Industrial Technology, Tokyo 1168523, Japan

4 Mechanical Engineering, Shonan Institute of Science, Kanagawa 2518511, Japan

5 Department of Mechanical Systems Engineering, Tokyo University of Agriculture and Technology, Tokyo 1848588, Japan

Elsinga et al. 2004; Bang and Lee 2013; Venkatakrishnan and Meier 2004; Nicolas et al. 2017; Ichihara et al. 2022; Yamamoto et al. 2022, 2015; Shimazaki et al. 2022; Hayasaka et al. 2016; Heineck et al. 2019; Hill and Haering 2017; Bauknecht et al. 2015; Mizukaki et al. 2014; Viola et al. 2021). However, the conventional BOS technique exhibits certain drawbacks, such as a lower measurement sensitivity than the conventional schlieren technique, and the measured phenomena are blurred owing to diverging light. Generally, the camera has to focus on the background image behind the target and, therefore, blurring is unavoidable. To reduce the blur, the aperture of the lens is usually adjusted to correspond to a larger f-number, and the background is placed close to the target so that they are both within the depth of field as much as possible (Leopold et al. 2006; Kaneko et al. 2021). As a result, the displacement of the background image becomes smaller (i.e., l_b in Eq. (1) is small), but this lowers the sensitivity. Several approaches have been reported to overcome this trade-off between blurring and sensitivity. For example, Leopold et al. proposed the colored background-oriented schlieren (CBOS) technique (Sourgen et al. 2012), and then they employ background projection to keep the background close to the model in the test section of a wind tunnel (Leopold et al. 2012). This places the background

within the depth of field of a normal camera lens. In addition, Ota et al. introduced a telecentric optical system to the BOS technique to improve the spatial resolution by collecting parallel projections of the background through the test section (Ota et al. 2015b). Furthermore, Ota et al. proposed the colored-grid background-oriented schlieren (CGBOS) technique which uses a colored-grid background, and the technique has been applied to some experiments (Ota et al. 2011, 2015a). Meier et al. proposed a BOS imaging technique that uses a conventional BOS set-up, a negative focus distance mode, a double-pass mode, and an in-focus target mode with laser speckle illumination (Meier and Roesgen 2013). The advantage of this technique is that there is no loss of sensitivity. However, the laser speckle is very sensitive, and the speckle pattern can be unsteady owing to temperature changes in the laser oscillator or slight deviations of the speckle screen. In addition, it is difficult to obtain sufficient brightness for high-speed imaging. Therefore, it is difficult to apply this technique to practical tests, such as wind-tunnel experiments.

In this study, to overcome the drawbacks of the conventional BOS technique and develop a practical visualization technique, a double-pass BOS (DPBOS) imaging system using a digital projector was introduced. The theoretical model and experimental results are presented below.

2 Optical set-up of DPBOS

Figure 1 shows the conventional BOS set-up (Venkatakrishnan and Meier 2004). If the refractive index of the medium between the background and the camera is changed, the background image is captured at the image sensor of the digital camera with a displacement of Δh. This displacement occurs because of the refraction of light passing through the schlieren object (using density gradients), as shown by the solid line in the figure. The relationship between the

displacement of the background Δh and the refractive index n is expressed by

$$\Delta h = \frac{l_b f}{l_b + l_c - f} \frac{1}{n_0} \int_{l_b - \Delta l_b}^{l_b + \Delta l_b} \frac{\partial n}{\partial r(x, y)} dl, \qquad (1)$$

where l_b is the distance between the background and the schlieren object, l_c is the distance between the camera and the schlieren object, f is the focal length of the camera, and n_0 is the reference refractive index (Meier 2002). The relationship between the density ρ and the refractive index n is given by the Gladstone–Dale equation, as follows:

$$n = \rho G + 1, \qquad (2)$$

where G is the Gladstone–Dale constant. In general, the camera should focus on the background, but this results in the measured phenomena appearing blurry, as mentioned above. The displacement of the background is usually as small as a few pixels on the sensor of the digital camera. This is one of the reasons why the sensitivity of the BOS is not higher than that of the conventional schlieren method, which uses the parallel light and corresponds to the case in which l_b is infinite. To increase the sensitivity of the conventional schlieren technique, the double-pass schlieren method (Payri et al. 2017) has been widely used in various applications. The double-pass schlieren method can measure the displacement with increased sensitivity because the distance between the schlieren object and the image sensor is larger than that in the conventional schlieren method. Therefore, in this study, the DPBOS was developed to increase the sensitivity of the conventional BOS.

The optical set-up of the DPBOS is shown in Fig. 2. The colored-grid background pattern is projected parallel to the test section (schlieren object) from a projector using a telecentric optical set-up consisting of a lens and a concave mirror (with focal length f_1). A prism was installed to observe the schlieren object using a digital camera from the

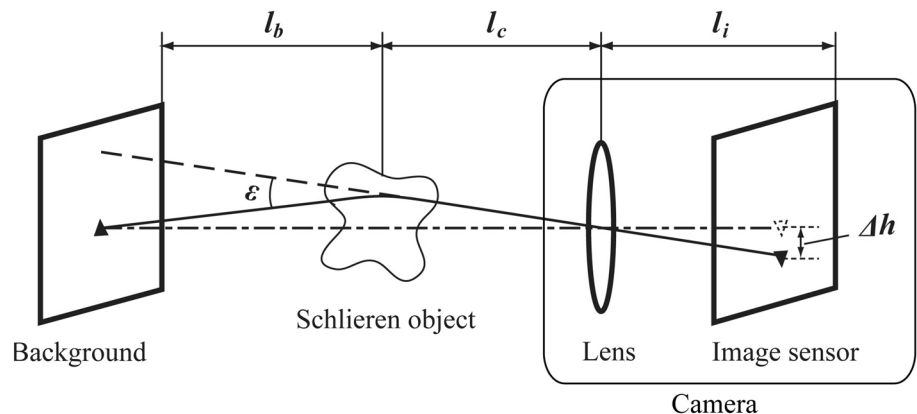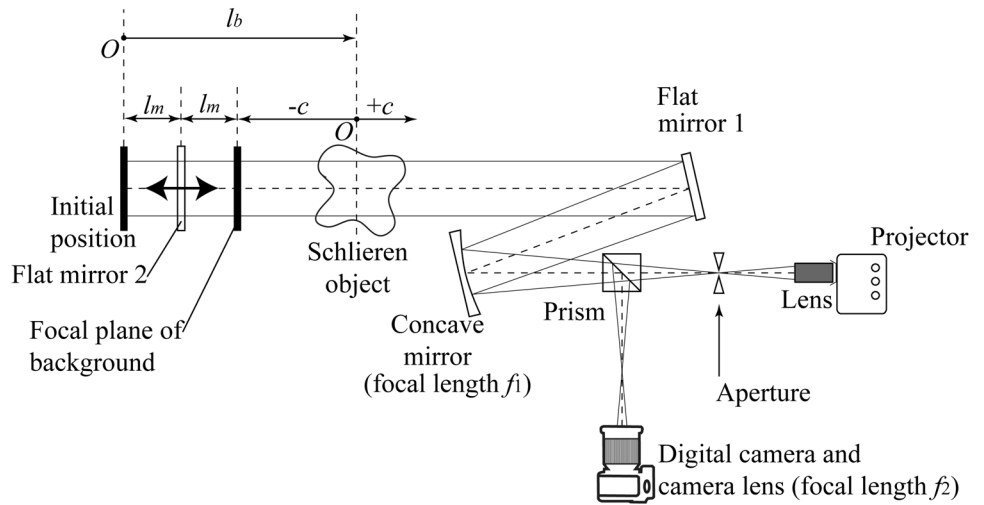**Fig. 1** Optical set-up for the conventional BOS

same optical axis as that of the background projection. The optical set-up of the camera was also telecentric, consisting of a concave mirror and a camera lens (with focal length f_2).

Figure 3 shows the geometry of the DPBOS. The parallel projected background pattern is focused on the initial position. The displacement at this position, $\Delta y\prime$, is expressed as follows:

$$\Delta y' = -l_b \frac{1}{n_0} \int_{l_b-\Delta l_b}^{l_b+\Delta l_b} \frac{\partial n}{\partial r(x,y)} dl. \qquad (3)$$

The displacement obtained with the DPBOS is opposite to that obtained by conventional BOS measurement.

When a mirror is installed at a distance l_m from the initial position, the projected background is reflected at the mirror and focused on to a position at a distance of

2 lm, as shown in Fig. 3. At the same time, the digital camera focuses on the focal position through a prism, and the projected background pattern can be captured as a real image using a telecentric BOS set-up (Ota et al. 2015b).

The displacement of the projected background pattern obtained with the telecentric BOS, $\Delta y''$, can be expressed as
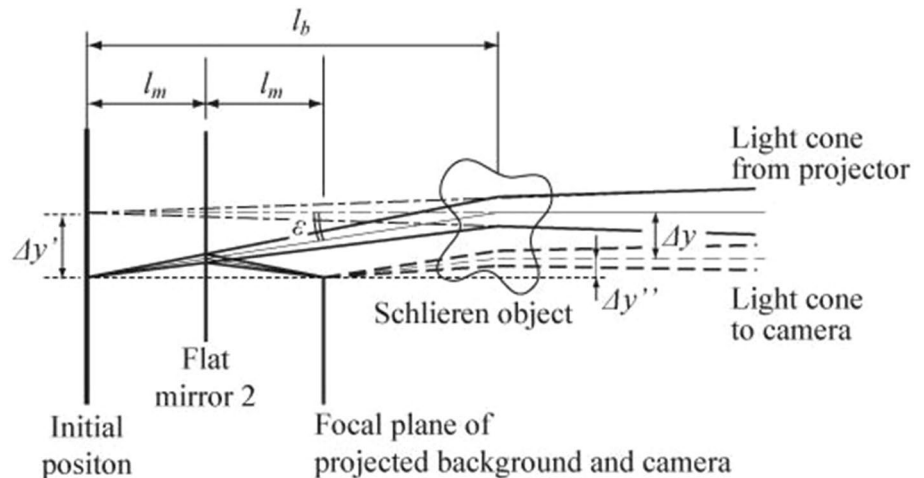
$$\Delta y'' = \left(l_b - 2l_m\right) \frac{1}{n_0} \int_{l_b-\Delta l_b}^{l_b+\Delta l_b} \frac{\partial n}{\partial r(x,y)} dl \qquad (4)$$

Hence, the total displacement Δy obtained with the DPBOS is

$$\Delta y = \Delta y' + \Delta y'' = -2l_m \frac{1}{n_0} \int_{l_b-\Delta l_b}^{l_b+\Delta l_b} \frac{\partial n}{\partial r(x,y)} dl, \qquad (5)$$

or

Fig. 3 Geometry of the DPBOS

$$\Delta y = -\left(l_b + c\right)\frac{1}{n_0}\int_{l_b-\Delta l_b}^{l_b+\Delta l_b}\frac{\partial n}{\partial r(x, y)}dl, \tag{6}$$

where c denotes the distance from the schlieren object to the focal plane of the projected background. The distance c is positive when the focal-plane position is located between the schlieren object and flat mirror 1. Conversely, c is negative when the focal-plane position is located between the schlieren object and flat mirror 2. The displacement at the image sensor of the camera, which is obtained via the magnitude of the telecentric optical system (Ota et al. 2015b), can be expressed as

$$\Delta h = \frac{f_2}{f_1}\Delta y, \tag{7}$$

where f_1 is the focal length of the concave mirror and f_2 is the focal length of the camera lens. Therefore, the final expression for the displacement at the image sensor of the camera is given as follows:

$$\Delta h = -\left(l_b + c\right)\frac{f_2}{f_1}\frac{1}{n_0}\int_{l_b-\Delta l_b}^{l_b+\Delta l_b}\frac{\partial n}{\partial r(x, y)}dl. \tag{8}$$

The depth of field of the telecentric BOS set-up Δl is given as (Ota et al. 2015b)

$$\Delta l = 2\delta\frac{F}{M} = 2\delta\frac{f_1/d}{f_2/f_1}, \tag{9}$$

where F denotes the f-number of the optical system, M is the magnitude of the telecentric BOS set-up, δ is the circle of the confusion diameter, and d is the diameter of the aperture.

3 Experiments

3.1 Preliminary experimental set-up and condition

The experimental set-up for the DPBOS measurement is shown in Fig. 4. The colored-grid background pattern consisting of horizontal green stripes and vertical red stripes was projected from the digital projector (Epson, EH-TW5200) with an achromatic doublet lens (Edmond, 63–701, focal length = 100 mm). This light was then passed through the schlieren object, reflected by a flat mirror 2, and passed through the schlieren object again. The projected background pattern was captured through a prism using a digital camera. A normal digital camera (Canon EOS Kiss Digital X3, 4752×3168 pixels CMOS sensor) with a telephoto lens (SIGMA 70–300 mm F4-5.6 DG MACRO) was used to record the projected background.
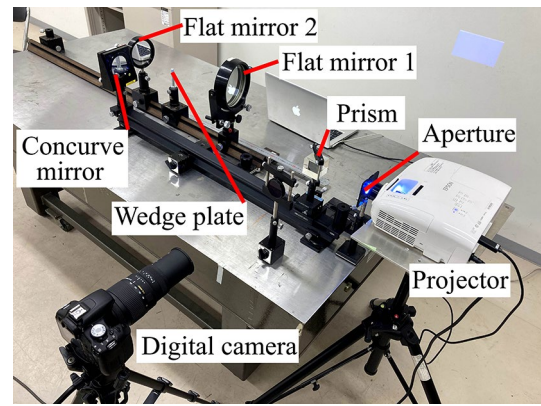
Fig. 4 Experimental set-up of the DPBOS measurement

The focal lengths of the concave mirror and of the camera lens were $f_1 = 1000$ mm and $f_2 = 300$ mm, respectively. An aperture of 5 mm was placed at the focal positions of both the concave mirror and the achromatic doublet lens. The distance from the concave mirror to the camera lens $(f_1 + f_2)$ was fixed at 1300 mm. Using Eq. (9) and the f-number of the optical system $(f = f_1/d = 200)$, the calculated depth of field Δl for the telecentric optical set-up of the camera was 21.9 mm, with a circle of confusion diameter of $\delta = 0.0328$ mm (Ota et al. 2015b). In this study, a wedge plate with a wedge angle of 1° (SIGUMAKOKI, WSB-30C05-10–1, material: BK7) was used as a schlieren object to evaluate the basic equation of the proposed DPBOS (Eq. (8)). An outline of the theoretical displacement of the proposed DPBOS is shown in Fig. 5. The projected background passed through a wedge at a refraction angle ε_1. Then, the projected background was reflected at a flat mirror and was focused on to the position marked with an asterisk (Fig. 5). The upper part of the figure shows the case for which $2\,lm < l_b$. This case is the same as that shown in Fig. 3. The lower part of the figure shows the case for which $2l_m \geqq l_b$. In this case, the projected background passed through the wedge twice, was refracted at an angle ε_2 and was then focused on to the focal position. The thickness of the wedge plate was 5 mm at the thinnest point and was sufficiently small compared to l_b. Therefore, the thickness of the wedge was neglected in this study. Using Snell's law and a BK7 refractive index of 1.517, the refractive indices ε_1 and ε_2 were calculated to be 0.519° and 1.038°, respectively.

In this experiment, the distance between the schlieren object and the initial position l_b was set to 350, 300, and 250 mm in three separate trials. The experimental conditions are listed in Table 1. The experimental procedure for adjusting the optical system when $l_b = 350$ mm was as follows. First, the projected background was focused on to the initial position by adjusting the position of the projector lens. Second, a flat mirror was placed at this position. This was

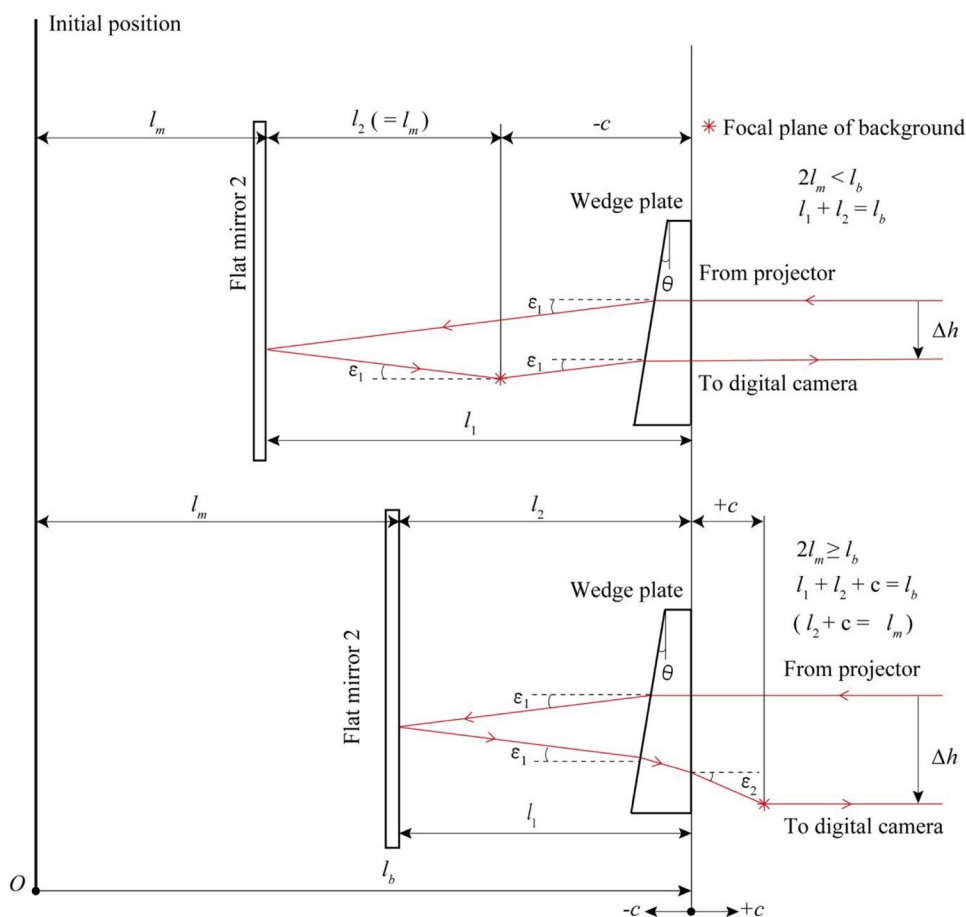**Fig. 5** Outline of theoretical displacement Δh

	l_b [mm]		
l_m [mm]	350	300	250
	0	0	0
	25	25	25
	50	50	50
	75	75	75
	100	100	100
	125	125	125
	150	150	150
	175	175	
	200	200	
	225		
	250		

Table 1 Experimental conditions

the case for $l_m = 0$ mm. The flat mirror was moved 25 mm toward the wedge plate according to the experimental conditions. The focal plane was moved 50 mm when flat mirror 2 was moved 25 mm. Therefore, this DPBOS set-up was in focus mode when $l_m = 175$ mm.

An example of the DPBOS image of the wedge plate for the case in which $l_b = 250$ mm and $l_m = 75$ mm is shown in Fig. 6a. In this figure, both the wedge plate and background image are in focus, and they are captured without any blurs, which is the advantage of the DPBOS technique. The quantitative displacement distribution is shown in Fig. 6b. The displacement inside the wedge plate was almost constant, at approximately 70 pixels.

The plot in Fig. 7 shows the experimental displacement data (Δh) and the theoretical displacement (Δh_t) predicted by Snell's law as a function of l_m. The dashed and dot-dashed lines in the figure also indicate the theoretical displacement values that incorporate the half length of depth of field $\Delta l/2$ in Eq. (9). This is because the depth of field Δl by Eq. (9) considers both negative and positive direction around initial position O in Fig. 5. The figure clearly demonstrates that Δh increases linearly with l_m. However, the experimental data were systematically lower than the theoretical values. This is because the focus of the camera lens was adjusted from a short range to a range of infinity. Nevertheless, the experimental results were distributed within the theoretical displacement values that incorporated the depth of field, and therefore, the experimental displacement data are in good agreement with the theoretical displacement. Furthermore, a wedge plate with a refraction angle of 0.519° was used for validation; in the actual case, the refraction angle becomes smaller by an order of magnitude, e.g., a candle plume
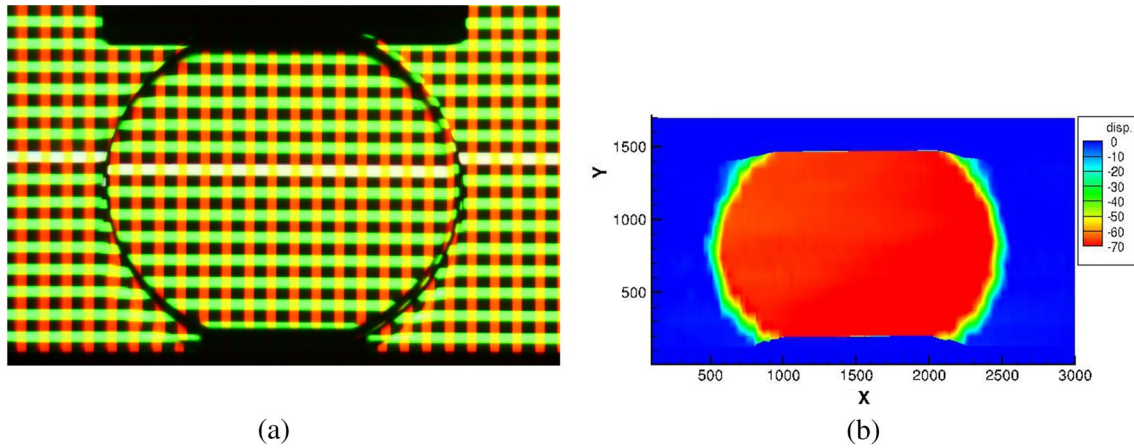
(a)   (b)

Fig. 6 Example of a DPBOS image (left) and its displacement (right) for $l_b = 250$ mm and $l_m = 75$ mm

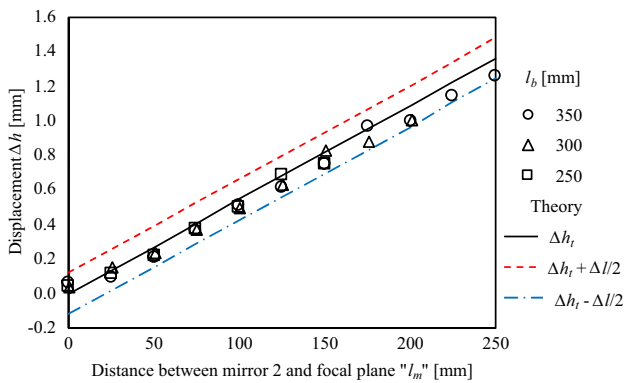**Fig. 7** Experimental (circles, triangles, and squares) and theoretical (lines) displacement data

of ~ 0.06° (Kafri 1980). This error would be too small to accurately evaluate with the image sensor of camera. Thus, the displacement of the DPBOS set-up can be obtained with sufficient accuracy using Eq. (8).

3.2 Measurement of the density field in the vicinity of a heat sink

The advantage of the DPBOS technique is that it is possible to set both the focal position of the projected background image and the camera simultaneously, and its position can be set at any location in the observation area. Therefore, it is possible to obtain a suitable displacement for image processing while focusing on both the background image and the measurement target. For a small density-change case, e.g., in a suction-type wind-tunnel test, it is possible to obtain a larger displacement by setting the focal position of the projected background image on the $+c$ side (Fig. 5, $2lm \geq l_b$) to obtain a larger displacement. However, the focal length of the telecentric optical system on the camera side is limited

to the vicinity of the focal position of the first lens (concave mirror in this report); this should be noted when setting up the DPBOS optical system.

An aluminum heat sink (fin height $H \times$ distance $D \times$ thickness t, $16 \times 25 \times 1$ mm^3, number of fins $n_f = 4$) was installed at the position of the wedge plate in Fig. 4 for verification. Figure 8a shows a DPBOS image taken with l_b and l_m set to 250 mm and 125 mm, respectively. The background image is a random dot pattern commonly used in the conventional BOS method. A pseudo-color image of the horizontal displacement obtained by OpenPIV (Liberzon et al. 2009) with an interrogation window size of 16×16 pixels with 50% overlap is shown in Fig. 8b. For comparison, a conventional BOS image taken with $l_b = 250$ mm, $l_c = 1050$ mm, and $f = 300$ mm, where the magnitude factor in Eq. (1) is set to be equal to that of DPBOS, is shown in Fig. 8c. The f-number of the camera is set to 29 to increase the focal depth. The background image was printed on to a transparent sheet and illuminated with a flashlight from the rear. It is clearly seen that using conventional BOS measurement, the camera is focused on the background image, and the heat sink located in the foreground is blurred and its detailed shape cannot be recognized. In contrast, the heat sink is accurately captured with DPBOS as shown in Fig. 8a. As discussed in previous reports (Ota et al. 2015b; Gojani et al. 2013), the blur can be revealed by a cone diameter of light ray at the position of aluminum heat sink. The cone diameter of DPBOS and conventional BOS is 0.11 mm and 17.3 mm, respectively. It means that the blur effect of DPBOS is extremely small compared to conventional BOS.

Figure 8e shows the displacement at the red line in the DPBOS and conventional BOS images. The red line is located 13 mm from the bottom of the heat sink; the vertical (black) dashed lines in Fig. 8e indicate the heat-sink surface. Comparing the pseudo-color of displacement in Fig. 8b and d shows that the overall density change can be captured even
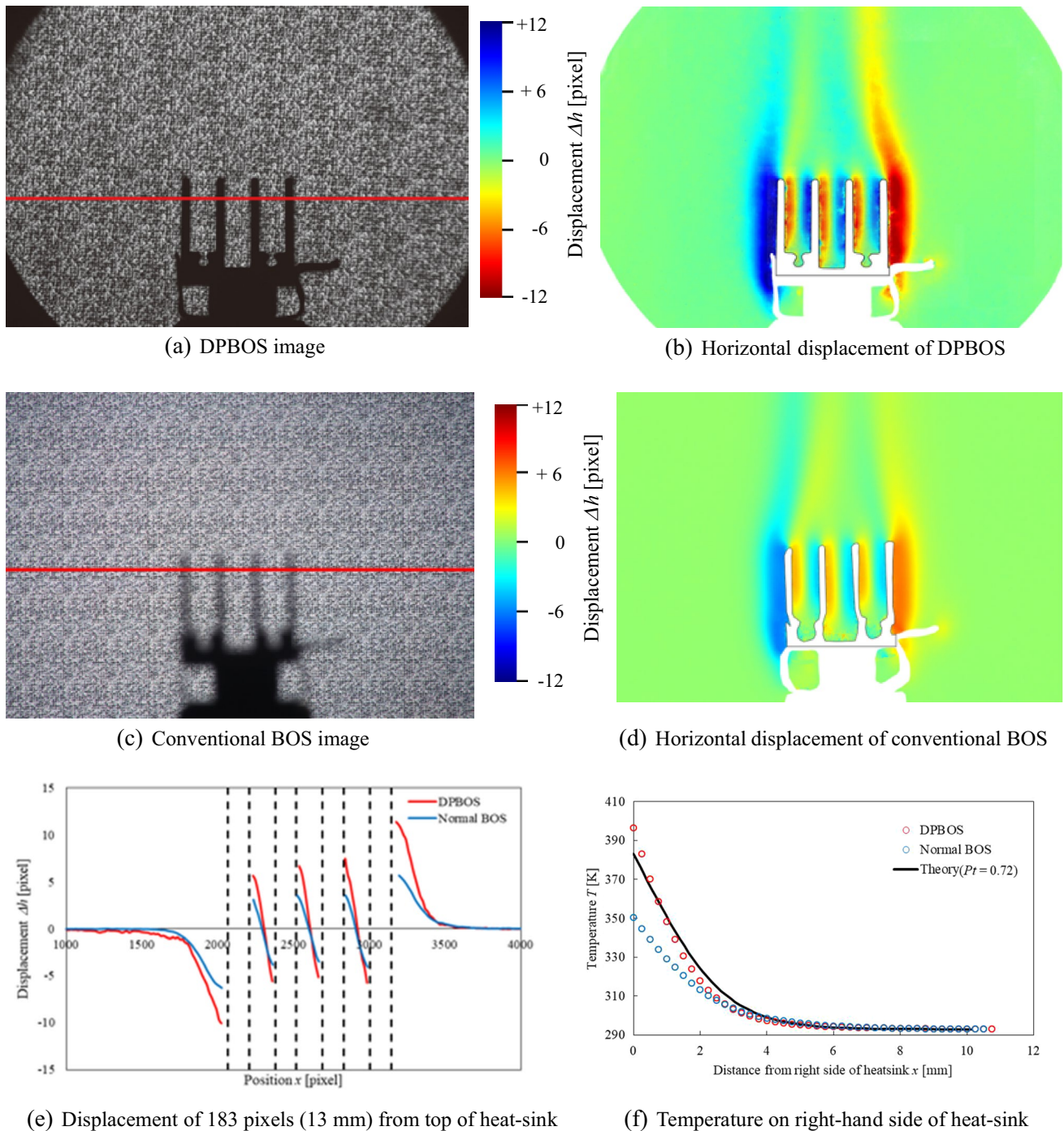
(a) DPBOS image

(b) Horizontal displacement of DPBOS

(c) Conventional BOS image

(d) Horizontal displacement of conventional BOS

(e) Displacement of 183 pixels (13 mm) from top of heat-sink

(f) Temperature on right-hand side of heat-sink

Fig. 8 Measurement of the density field in the vicinity of a heat sink

with conventional BOS, but with DPBOS it is possible to observe the density change on the heat-sink surface in more detail, as shown in Fig. 8e.

In order to evaluate the proposed DPBOS measurement, the resultant temperature distributions in the normal direction on the right-hand side surface of the heat sink, obtained from DPBOS and conventional BOS, are compared with the

theoretical temperature distribution in the boundary layer of laminar-free convection around the plate. First, the density-gradient distribution was calculated from Eqs. (1) and (8) using the displacement data obtained by each BOS method. Second, the density ratio (ρ / ρ_0) was calculated by integration of the density gradient. Finally, the temperature distribution was obtained from the equation of state at atmospheric

conditions. The initial density, ρ_0, was set to 1.205 kg/m^3 at room temperature (293 K), and the Gladstone–Dale constant was 2.226×10^{-4}. The theoretical value was calculated from the dimensionless temperature $H(\eta)$ of Eq. (10). The similarity parameter η and the Grashof number Gr are given by Eqs. (11) and (12), respectively, where x is the perpendicular distance from the plate surface, y is distance from the bottom of the heat sink, g is the gravitational acceleration, T_p is the heat-sink surface temperature, T_∞ is the free-stream air temperature, ν is the kinematic viscosity of air, and β is the coefficient of thermal expansion of air (Hargather and Settles 2012). The theoretical temperature distribution around the heat sink in air at the position of $y = 13$ mm was calculated from table of Ostrach (Ostrach 1952), with the Prandtl number $Pr = 0.72$. The surface temperature of the heat sink T_p was set to 383 K, and it was monitored by infrared camera during the experiments.

$$H = \frac{T - T_\infty}{T_p - T_\infty} \qquad (10)$$

$$\eta = \left(\frac{Gr}{4}\right)^{1/4} \frac{x}{y} \qquad (11)$$

$$Gr = \frac{g\beta(T_p - T_\infty)}{\nu^2} \qquad (12)$$

Figure 8f shows the resultant temperature distribution. The DPBOS result shows good agreement with the theoretical value, while the estimated temperature from the conventional BOS measurement was lower than the theoretical value, especially in the region where the distance from the wall was less than 3 mm. This is considered to be the effect of the blur owing to defocus. The temperature near the heat-sink surface was 350 K for the conventional BOS and 396 K for the DPBOS, with errors of 9% and 3%, respectively. The estimated temperature was 13 K higher for the DPBOS result, but this is due to the use of a random dot pattern in the background image and the influence of the interrogation window size in calculating the displacement around the surface. The proposed method clearly shows the advantage of DPBOS over BOS in overcoming the defocus problem and achieving high-accuracy measurements.

4 Conclusion

To overcome the drawbacks of the conventional BOS technique, a DPBOS method, using a digital projector, is proposed and its basic formula is confirmed. In the conventional BOS technique, if l_b is increased to increase the displacement, the influence of blur becomes large, but in the proposed DPBOS technique, even if l_b is large, measurement can be performed, while the camera focuses on the measurement target, with high accuracy and sensitivity. Since the focal position of the projected background image and the camera can be set to any position in the test field, it is expected that the proposed DPBOS can be applied to various experiments. The disadvantages of the DPBOS are that the measurable size is limited by the diameter of the optical components, and the optical system is rather complicated. Furthermore, some efforts are required to set up the system compared to conventional BOS. However, regarding experiments in wind tunnels, the schlieren optical system suitable for the size of the wind tunnel has been generally installed; quantitative density measurement with high accuracy and sensitivity can be achieved by assembling DPBOS set-up from these optical systems. Using a digital projector means that high-brightness photography can be achieved at low cost, which is very advantageous for measurements made using a high-speed camera. Furthermore, it is possible to realize quantitative density measurement in the flow field, including the area in the vicinity of the model surface, which is not possible using the conventional BOS technique.

Data availability Not applicable.

Declarations

Conflict of interest Not applicable.

Ethical approval Not applicable.

References

Bang SH, Lee CS (2013) Comparison between background oriented Schlieren (BOS) technique and scattering method for the spray characteristics of evaporating oxygenated fuels. Optik 124(15):2147–2150

Bauknecht A, Ewers B, Wolf C, Leopold F, Yin J, Raffel M (2015) Three-dimensional reconstruction of helicopter blade–tip vortices using a multi-camera BOS system. Exp Fluids 56(1):1–13

Elsinga GE, Van Oudheusden BW, Scarano F, Watt DW (2004) Assessment and application of quantitative schlieren methods: Calibrated color schlieren and background oriented schlieren. Exp Fluids 36(2):309–325

Gojani AB, Kamishi B, Obayashi S (2013) Measurement sensitivity and resolution for background oriented schlieren during image recording. J Visualization 16:201–207

Hargather MJ, Settles GS (2012) A comparison of three quantitative schlieren techniques. Opt Lasers Eng 50(1):8–17

Hayasaka K, Tagawa Y, Liu T, Kameda M (2016) Optical-flow-based background-oriented schlieren technique for measuring a laser-induced underwater shock wave. Exp Fluids 57:179

Heineck TJ, Banks WD, Schairer TE, Bean SP, Haering AE, Pauer AB, Martin JB, and Larson ND (2019) Air-to-air background oriented schlieren technique, U.S. pat. 10,169,847

Hill MA, Haering EA (2017) Flow visualization of aircraft in flight by means of Background Oriented Schlieren using Celestial Objects. *In: 33rd AIAA Aerodynamic Measurement Technology and Ground Testing Conference*, pp. 3553

Ichihara S, Shimazaki T, Tagawa Y (2022) Background-oriented schlieren technique with vector tomography for measurement of axisymmetric pressure fields of laser-induced underwater shock waves. Exp Fluids 63:182

Kafri O (1980) Noncoherent method for mapping phase objects. Opt Lett 5:555–557

Kaneko Y, Nishida H, Tagawa Y (2021) Background-oriented-schlieren measurement of near-surface density field in surface dielectric-barrier-discharge. Meas Sci Technol 32:125402

Leopold F, Simon J, Gruppi D and Schäfer HJ (2006) Recent improvements of the back-ground oriented schlieren technique (BOS) by using a colored background. Proc. 12th ISFV, Göttingen, Germany, ISFV12–3.4, pp 1–10.

Leopold F, Jagusinski F, Demeautis C, Ota M, and Klatt D (2012) Increase of accuracy for CBOS by background projection. In: Proceedings of 15th international symposium on flow visualization (ISFV15–087), Minsk, Belarus.

Liberzon A, Gurka R, and Taylor Z (2009) OpenPIV Home Page http://www.openpiv.net

Meier GEA (2002) Computerized background-oriented schlieren. Exp Fluids 33:181–187

Meier AH, Roesgen T (2013) Improved background oriented schlieren imaging using laser speckle illumination. Exp Fluids 54(6):1549

Mizukaki T, Wakabayashi K, Matsumura T, Nakayama K (2014) Background-oriented schlieren with natural background for quantitative visualization of open-air explosions. Shock Waves 24(1):69–78

Nicolas F, Donjat D, Plyer A, Champagnat F, Le Besnerais G, Micheli F, Cornic P, Le Sant Y, Deluc JM (2017) Experimental study of a co-flowing jet in ONERA's F2 research wind tunnel by 3D background oriented schlieren. Meas Sci Technol 28(8):085302

Ostrach S (1952) An analysis of laminar free-convection flow and heat transfer about a flat plate parallel to the direction of the generating body force. National Aeronautics and Space Administration Cleveland Ohio Lewis Research Center.

Ota M, Hamada K, Kato H, Maeno K (2011) Computed-tomographic density measurement of supersonic flow field by colored-grid background oriented schlieren (CGBOS) technique. Meas Sci Technol 22:1–7

Ota M, Kurihara K, Aki K, Miwa Y, Inage T, Maeno K (2015a) Quantitative density measurement of the lateral jet / cross flow interaction field by colored-grid background oriented schlieren (CGBOS) technique. J Visualization 18(3):543–552

Ota M, Leopold F, Noda R, Maeno K (2015b) Improvement in spatial resolution of background oriented schlieren technique by introducing a telecentric optical system and its application to supersonic flow. Exp Fluids 56(48):1–10

Payri R, Salvador FJ, Bracho G, Viera, (2017) Differences between single and double-pass schlieren imaging on diesel vapor spray characteristics. Appl Therm Eng 125:220–231

Raffel M (2015) Background-oriented schlieren (BOS) techniques. Exp Fluids 56(3):60

Shimazaki T, Ichihara S, Tagawa Y (2022) Background oriented schlieren technique with fast Fourier demodulation for measuring large density-gradient fields of fluids. Exp Thermal Fluid Sci 134:110598

Sourgen F, Leopold F, Klatt D (2012) Reconstruction of the density field using the colored background oriented schlieren technique (CBOS). Opt Lasers Eng 50(1):29–38

Venkatakrishnan L, Meier GEA (2004) Density measurements using the background oriented Schlieren technique. Exp Fluids 37:237–247

Viola M et al (2021) Face coverings, aerosol dispersion and mitigation of virus transmission risk. IEEE Open J Eng Med Biol 2:26–35. https://doi.org/10.1109/OJEMB.2021.3053215

Yamamoto S, Tagawa Y, Kameda M (2015) Application of background-oriented schlieren (BOS) technique to a laser-induced underwater shock wave. Exp Fluids 56(5):93

Yamamoto S, Shimazaki T, Franco-Gomez A, Ichihar S, Yee J, Tagawa Y (2022) Contactless pressure measurement of an underwater shock wave in a microtube using a high-resolution background-oriented schlieren technique. Exp Fluids 63:142